Measurements of inclusive semileptonic branching fractions of b hadrons in Z^0 decays

The OPAL Collaboration

G. Abbiendi[2], K. Ackerstaff[8], G. Alexander[23], J. Allison[16], N. Altekamp[5], K.J. Anderson[9], S. Anderson[12], S. Arcelli[17], S. Asai[24], S.F. Ashby[1], D. Axen[29], G. Azuelos[18,a], A.H. Ball[8], E. Barberio[8], R.J. Barlow[16], J.R. Batley[5], S. Baumann[3], J. Bechtluft[14], T. Behnke[27], K.W. Bell[20], G. Bella[23], A. Bellerive[9], S. Bentvelsen[8], S. Bethke[14], S. Betts[15], O. Biebel[14], A. Biguzzi[5], I.J. Bloodworth[1], P. Bock[11], J. Böhme[14], D. Bonacorsi[2], M. Boutemeur[33], S. Braibant[8], P. Bright-Thomas[1], L. Brigliadori[2], R.M. Brown[20], H.J. Burckhart[8], P. Capiluppi[2], R.K. Carnegie[6], A.A. Carter[13], J.R. Carter[5], C.Y. Chang[17], D.G. Charlton[1,b], D. Chrisman[4], C. Ciocca[2], P.E.L. Clarke[15], E. Clay[15], I. Cohen[23], J.E. Conboy[15], O.C. Cooke[8], J. Couchman[15], C. Couyoumtzelis[13], R.L. Coxe[9], M. Cuffiani[2], S. Dado[22], G.M. Dallavalle[2], R. Davis[30], S. De Jong[12], A. de Roeck[8], P. Dervan[15], K. Desch[27], B. Dienes[32,h], M.S. Dixit[7], J. Dubbert[33], E. Duchovni[26], G. Duckeck[33], I.P. Duerdoth[16], P.G. Estabrooks[6], E. Etzion[23], F. Fabbri[2], A. Fanfani[2], M. Fanti[2], A.A. Faust[30], L. Feld[10], F. Fiedler[27], M. Fierro[2], I. Fleck[10], A. Frey[8], A. Fürtjes[8], D.I. Futyan[16], P. Gagnon[7], J.W. Gary[4], G. Gaycken[27], C. Geich-Gimbel[3], G. Giacomelli[2], P. Giacomelli[2], V. Gibson[5], W.R. Gibson[13], D.M. Gingrich[30,a], D. Glenzinski[9], J. Goldberg[22], W. Gorn[4], C. Grandi[2], K. Graham[28], E. Gross[26], J. Grunhaus[23], M. Gruwé[27], C. Hajdu[31] G.G. Hanson[12], M. Hansroul[8], M. Hapke[13], K. Harder[27], A. Harel[22], C.K. Hargrove[7], M. Harin-Dirac[4], M. Hauschild[8], C.M. Hawkes[1], R. Hawkings[27], R.J. Hemingway[6], G. Herten[10], R.D. Heuer[27], M.D. Hildreth[8], J.C. Hill[5], P.R. Hobson[25], A. Hocker[9], K. Hoffman[8], R.J. Homer[1], A.K. Honma[28,a], D. Horváth[31,c], K.R. Hossain[30], R. Howard[29], P. Hüntemeyer[27], P. Igo-Kemenes[11], D.C. Imrie[25], K. Ishii[24], F.R. Jacob[20], A. Jawahery[17], H. Jeremie[18], M. Jimack[1], C.R. Jones[5], P. Jovanovic[1], T.R. Junk[6], N. Kanaya[24], J. Kanzaki[24], D. Karlen[6], V. Kartvelishvili[16], K. Kawagoe[24], T. Kawamoto[24], P.I. Kayal[30], R.K. Keeler[28], R.G. Kellogg[17], B.W. Kennedy[20], D.H. Kim[19], A. Klier[26], T. Kobayashi[24], M. Kobel[3,d], T.P. Kokott[3], M. Kolrep[10], S. Komamiya[24], R.V. Kowalewski[28], T. Kress[4], P. Krieger[6], J. von Krogh[11], T. Kuhl[3], P. Kyberd[13], G.D. Lafferty[16], H. Landsman[22], D. Lanske[14], J. Lauber[15], I. Lawson[28], J.G. Layter[4], D. Lellouch[26], J. Letts[12], L. Levinson[26], R. Liebisch[11], B. List[8], C. Littlewood[5], A.W. Lloyd[1], S.L. Lloyd[13], F.K. Loebinger[16], G.D. Long[28], M.J. Losty[7], J. Lu[29], J. Ludwig[10], D. Liu[12], A. Macchiolo[18], A. Macpherson[30], W. Mader[3], M. Mannelli[8], S. Marcellini[2], A.J. Martin[13], J.P. Martin[18], G. Martinez[17], T. Mashimo[24], P. Mättig[26], W.J. McDonald[30], J. McKenna[29], E.A. Mckigney[15], T.J. McMahon[1], R.A. McPherson[28], F. Meijers[8], P. Mendez-Lorenzo[33], F.S. Merritt[9], H. Mes[7], A. Michelini[2], S. Mihara[24], G. Mikenberg[26], D.J. Miller[15], W. Mohr[10], A. Montanari[2], T. Mori[24], K. Nagai[8], I. Nakamura[24], H.A. Neal[12,g], R. Nisius[8], S.W. O'Neale[1], F.G. Oakham[7], F. Odorici[2], H.O. Ogren[12], A. Okpara[11], M.J. Oreglia[9], S. Orito[24], G. Pásztor[31], J.R. Pater[16], G.N. Patrick[20], J. Patt[10], R. Perez-Ochoa[8], S. Petzold[27], P. Pfeifenschneider[14], J.E. Pilcher[9], J. Pinfold[30], D.E. Plane[8], P. Poffenberger[28], B. Poli[2], J. Polok[8], M. Przybycień[8,e], A. Quadt[8], C. Rembser[8], H. Rick[8], S. Robertson[28], S.A. Robins[22], N. Rodning[30], J.M. Roney[28], S. Rosati[3], K. Roscoe[16], A.M. Rossi[2], Y. Rozen[22], K. Runge[10], O. Runolfsson[8], D.R. Rust[12], K. Sachs[10], T. Saeki[24], O. Sahr[33], W.M. Sang[25], E.K.G. Sarkisyan[23], C. Sbarra[29], A.D. Schaile[33], O. Schaile[33], P. Scharff-Hansen[8], J. Schieck[11], S. Schmitt[11], A. Schöning[8], M. Schröder[8], M. Schumacher[3], C. Schwick[8], W.G. Scott[20], R. Seuster[14], T.G. Shears[8], B.C. Shen[4], C.H. Shepherd-Themistocleous[5], P. Sherwood[15], G.P. Siroli[2], A. Sittler[27], A. Skuja[17], A.M. Smith[8], G.A. Snow[17], R. Sobie[28], S. Söldner-Rembold[10,f], S. Spagnolo[20], M. Sproston[20], A. Stahl[3], K. Stephens[16], J. Steuerer[27], K. Stoll[10], D. Strom[19], R. Ströhmer[33], B. Surrow[8], S.D. Talbot[1], P. Taras[18], S. Tarem[22], R. Teuscher[9], M. Thiergen[10], J. Thomas[15], M.A. Thomson[8], E. Torrence[8], S. Towers[6], I. Trigger[18], Z. Trócsányi[32], E. Tsur[23], M.F. Turner-Watson[1], I. Ueda[24], R. Van Kooten[12], P. Vannerem[10], M. Verzocchi[8], H. Voss[3], F. Wäckerle[10], A. Wagner[27], C.P. Ward[5], D.R. Ward[5], P.M. Watkins[1], A.T. Watson[1], N.K. Watson[1], P.S. Wells[8], N. Wermes[3], D. Wetterling[11] J.S. White[6], G.W. Wilson[16], J.A. Wilson[1], T.R. Wyatt[16], S. Yamashita[24], V. Zacek[18], D. Zer-Zion[8]

[1]School of Physics and Astronomy, University of Birmingham, Birmingham B15 2TT, UK
[2]Dipartimento di Fisica dell' Università di Bologna and INFN, 40126 Bologna, Italy
[3]Physikalisches Institut, Universität Bonn, 53115 Bonn, Germany
[4]Department of Physics, University of California, Riverside CA 92521, USA
[5]Cavendish Laboratory, Cambridge CB3 0HE, UK
[6]Ottawa-Carleton Institute for Physics, Department of Physics, Carleton University, Ottawa, Ontario K1S 5B6, Canada
[7]Centre for Research in Particle Physics, Carleton University, Ottawa, Ontario K1S 5B6, Canada
[8]CERN, European Organisation for Particle Physics, 1211 Geneva 23, Switzerland

[9]Enrico Fermi Institute and Department of Physics, University of Chicago, Chicago IL 60637, USA
[10]Fakultät für Physik, Albert Ludwigs Universität, 79104 Freiburg, Germany
[11]Physikalisches Institut, Universität Heidelberg, 69120 Heidelberg, Germany
[12]Indiana University, Department of Physics, Swain Hall West 117, Bloomington IN 47405, USA
[13]Queen Mary and Westfield College, University of London, London E1 4NS, UK
[14]Technische Hochschule Aachen, III Physikalisches Institut, Sommerfeldstrasse 26-28, 52056 Aachen, Germany
[15]University College London, London WC1E 6BT, UK
[16]Department of Physics, Schuster Laboratory, The University, Manchester M13 9PL, UK
[17]Department of Physics, University of Maryland, College Park, MD 20742, USA
[18]Laboratoire de Physique Nucléaire, Université de Montréal, Montréal, Quebec H3C 3J7, Canada
[19]University of Oregon, Department of Physics, Eugene OR 97403, USA
[20]CLRC Rutherford Appleton Laboratory, Chilton, Didcot, Oxfordshire OX11 0QX, UK
[22]Department of Physics, Technion-Israel Institute of Technology, Haifa 32000, Israel
[23]Department of Physics and Astronomy, Tel Aviv University, Tel Aviv 69978, Israel
[24]International Centre for Elementary Particle Physics and Department of Physics, University of Tokyo, Tokyo 113-0033, and Kobe University, Kobe 657-8501, Japan
[25]Institute of Physical and Environmental Sciences, Brunel University, Uxbridge, Middlesex UB8 3PH, UK
[26]Particle Physics Department, Weizmann Institute of Science, Rehovot 76100, Israel
[27]Universität Hamburg/DESY, II Institut für Experimental Physik, Notkestrasse 85, 22607 Hamburg, Germany
[28]University of Victoria, Department of Physics, P O Box 3055, Victoria BC V8W 3P6, Canada
[29]University of British Columbia, Department of Physics, Vancouver BC V6T 1Z1, Canada
[30]University of Alberta, Department of Physics, Edmonton AB T6G 2J1, Canada
[31]Research Institute for Particle and Nuclear Physics, 1525 Budapest, P O Box 49, Hungary
[32]Institute of Nuclear Research, 4001 Debrecen, P O Box 51, Hungary
[33]Ludwigs-Maximilians-Universität München, Sektion Physik, Am Coulombwall 1, 85748 Garching, Germany

Abstract. A measurement of inclusive semileptonic branching fractions of b hadrons produced in Z^0 decays is presented. An enriched $Z^0 \to b\bar{b}$ sample is obtained with a lifetime flavour-tagging technique. The leptonic events are then selected from this sample, and classified according to their origin, which is determined by comparing the distribution of several kinematic variables using artificial neural network techniques. Using 3.6 million multihadronic events collected with the OPAL detector at energies near the Z^0 resonance, the values

$$\mathrm{BR}(\mathrm{b} \to \ell \mathrm{X}) = (10.84 \pm 0.09 \text{ (stat.)} \pm 0.21 \text{ (syst.)} \, ^{+0.21}_{-0.13} \text{ (model))}$$

$$\mathrm{BR}(\mathrm{b} \to \mathrm{c} \to \ell \mathrm{X}) = (\ 8.39 \pm 0.15 \text{ (stat.)} \pm 0.22 \text{ (syst.)} \, ^{+0.33}_{-0.29} \text{ (model))}.$$

are measured, where b denotes all weakly decaying b hadrons and ℓ represents either e or μ. The second error includes all experimental systematic uncertainties whereas the last error is due to uncertainties in modelling of the lepton momentum spectrum in semileptonic decays and b quark fragmentation. The average fraction of the beam energy carried by the weakly decaying b hadron, $\langle x_E \rangle$, is measured to be

$$\langle x_E \rangle = 0.709 \pm 0.003 \text{ (stat.)} \pm 0.003 \text{ (syst.)} \pm 0.013 \text{ (model)}$$

where the modelling error is dominated by the choice of b fragmentation model. The agreement between data and various semileptonic decay models and fragmentation functions is also investigated.

1 Introduction

Measurements of the semileptonic branching fraction of b hadrons are important in testing our understanding of the dynamics of heavy quark physics and are also important inputs for other b physics analyses. These measurements can also be used to extract the CKM matrix element V_{cb}. Recent QCD calculations which include higher-order perturbative corrections [1,2] have lowered the predicted value of the semileptonic branching ratio for B mesons, BR^B_{SL}, and now adequately reproduce the experimental results [3]. These calculations also predict a value for $\langle n_c \rangle$, the average number of charmed hadrons produced per B

---

[a] and at TRIUMF, Vancouver, Canada V6T 2A3
[b] and Royal Society University Research Fellow
[c] and Institute of Nuclear Research, Debrecen, Hungary
[d] on leave of absence from the University of Freiburg
[e] and University of Mining and Metallurgy, Cracow
[f] and Heisenberg Fellow
[g] now at Yale University, Dept of Physics, New Haven, USA
[h] and Depart of Experimental Physics, Lajos Kossuth University, Debrecen, Hungary.

meson decay, which is consistent with experimental data [2].

While theoretical calculations are now in better agreement with experiment, the measurements of BR_{SL} obtained at the $\Upsilon(4S)$ and Z^0 resonances have slightly disagreed for some time. The semileptonic branching fraction for B mesons has been measured at the $\Upsilon(4S)$ resonance to be $BR_{SL}^B = (10.45 \pm 0.21)\%$ [3], whereas a combination of all results obtained at the Z^0 resonance gives $BR_{SL}^b = (10.99 \pm 0.23)\%$ [3], where the superscript b indicates that the high energy data correspond to a mixture of $B^\pm$, B^0, B_s and b baryons, as opposed to $B^\pm$ and B^0 only at the $\Upsilon(4S)$ resonance. Assuming the semileptonic width, Γ_{sl}, to be the same for all b hadrons, as suggested by the result of [4], and given that the semileptonic branching ratio is related to the lifetimes, τ, by $BR_{SL} = \Gamma_{sl}/\Gamma_{total} = \tau \Gamma_{sl}$, one obtains

$$BR_{SL}^B = \frac{\tau_B}{\tau_b} \cdot BR_{SL}^b. \tag{1}$$

To remove the difference between the $\Upsilon(4S)$ and Z^0 results would require that τ_B/τ_b be 0.948, whereas current lifetime measurements yield τ_B/τ_b greater than one [3]. After applying the correction factor τ_B/τ_b, there is a difference of about two standard deviations between the $\Upsilon(4S)$ and Z^0 results for the branching fractions.

This paper describes the measurement of the semileptonic branching fraction for all b hadrons produced at or near the Z^0 resonance using identified electrons and muons in an enriched $Z^0 \rightarrow b\bar{b}$ sample. The measurement differs from previously published measurements [6–9] in the use of a method designed specifically to achieve a precise determination of the semileptonic branching ratios rather than extracting them from a multi-dimensional fit for several electroweak parameters. The dependence on the semileptonic decay models has been substantially reduced and the correlation with the R_b measurement eliminated. The analysis also allows the determination of $BR(b \rightarrow c \rightarrow \ell X)$ and $\langle x_E \rangle$, the mean fraction of beam energy carried by the weakly decaying b hadron, both of which are important inputs needed for other heavy flavour measurements, such as those described in [5]. The agreement between data and various semileptonic decay models and fragmentation functions is investigated in the Appendix.

2 The OPAL detector, data and Monte Carlo samples

The OPAL detector is described in reference [10]. The central tracking system is composed of a silicon microvertex detector, a precision vertex drift chamber, and a large-volume jet chamber surrounded by a set of drift chambers that measure the z-coordinate.[1] Charged particles

are identified by their specific energy loss, dE/dx, in the jet chamber gas. Further information on the performance of the tracking and dE/dx measurements can be found in reference [11]. These detectors are located inside a solenoid providing a magnetic field of 0.435 T. Outside the solenoid are a time-of-flight scintillator array and a lead-glass electromagnetic calorimeter with a presampler. Including the endcap electromagnetic calorimeters, the lead-glass blocks cover the range $|\cos\theta| < 0.98$. The next layer is the hadron calorimeter, consisting of the instrumented return yoke of the magnet. Finally, the detector is covered by several layers of muon chambers. In total, at least seven, and in most regions eight, absorption lengths of material lie between the interaction point and the muon detectors. This material is sufficient to absorb low-momentum muons produced at the vertex, but most muons with momenta above $2\,GeV/c$ reach the muon detectors. The muon chambers are constructed as two different detector subsystems in the barrel and endcap; together, they cover 93% of the full solid angle.

This analysis uses events recorded at centre-of-mass energies within $3\,GeV$ of the Z^0 peak during the $1992 - 1995$ running period when the silicon microvertex detector was fully operational. A total of 7.15 million multihadronic Monte Carlo events, and 4.88 and 1.93 million simulated $b\bar{b}$ and $c\bar{c}$ hadronic decays are also analysed. All samples were produced with the JETSET 7.4 Monte Carlo generator [12], with the fragmentation function of Peterson et al. [13] for heavy quarks. The ACCMM model [14] tuned to the CLEO data [15] is used to describe the lepton momentum spectrum in $b \rightarrow \ell$ and $b \rightarrow c \rightarrow \ell$ decays, as described in [16]. The Monte Carlo parameters were tuned to describe the OPAL data [17]. All simulated events were passed through the full OPAL detector simulation package [18].

3 Event selection and analysis method

Standard hadronic event selection [19] and detector performance requirements are applied to select a sample of 3.35 million events where the primary vertex can be reconstructed. Each event is divided into two hemispheres by the plane perpendicular to the thrust axis and containing the interaction point. The thrust value of the event is required to be greater than 0.8 to suppress contributions from events containing more than two jets, for example from hard gluon radiation or events with gluon splitting into a heavy quark pair. The polar angle of the thrust axis, θ_{th}, must satisfy $|\cos\theta_{th}| < 0.75$, to ensure that the event is contained within the central barrel region. A total of 2.15 million events satisfy these requirements.

Lifetime tagging techniques are used to suppress the contributions from non-$b\bar{b}$ events. Hemispheres are tagged as containing b hadrons ("b-tagged") using a neural network algorithm [20]. A cut is applied to the network output, selecting a sample of b-hemispheres with a purity

---

[1] The coordinate system is defined such that the z-axis follows the electron beam direction and the x-axis points towards the centre of the LEP ring. The polar angle θ is defined relative

to the $+z$-axis, and the azimuthal angle ϕ is defined relative to the $+x$-axis.

of 92 % and an efficiency of 30 %. The b purity for the hemisphere b-tag is extracted directly from the data, as detailed in the next section.

A search for lepton candidates is made in the hemisphere opposite a b-tagged hemisphere in events containing one or two such hemispheres. By using leptons found in the hemisphere opposite the b-tagged hemisphere rather than in the b-tagged hemisphere itself, a sample is obtained which does not bias the relative fraction of the different b hadron species. In addition, this method avoids introducing significant correlations between b flavour tagging and lepton selection.

Jets are formed from charged tracks and electromagnetic energy clusters unassociated with tracks using a cone algorithm [21], with a minimum energy of 5 GeV and a cone radius of 550 mrad. Jet shape and momentum variables are used in two neural networks, $NN_{b\ell}$ and $NN_{bc\ell}$, trained respectively to distinguish direct decays, $b \to \ell$, and cascade decays, $b \to c \to \ell$, from all other lepton sources, collectively termed as backgrounds. Separate neural networks are trained for electrons and muons. Details of the training of these neural networks are given in Sect. 4.1. The distributions of the neural network outputs are compared for the data and the Monte Carlo to determine the fractions of events from $b \to \ell$ and $b \to c \to \ell$ decays. Contributions from direct $c \to \ell$ decays are suppressed by the b-tagging requirement.

To determine the fraction of leptons coming from $B \to \ell$ and $b \to c \to \ell$ decays, a binned log-likelihood fit is performed which uses the shapes of the distributions of the neural network output variables. The fit also yields $\langle x_E \rangle$. The number of $b \to \ell$ and $b \to c \to \ell$ decays is obtained by multiplying the fitted fractions by the number of selected leptons, corrected by the lepton detection efficiencies, derived from Monte Carlo. Dividing the numbers of $b \to \ell$ and $b \to c \to \ell$ candidates by the number of b-flavoured hemispheres yields the branching ratios $BR(b \to \ell X)$ and $BR(b \to c \to \ell X)$. The number of b-flavoured hemispheres is extracted from the data using a double tagging technique.

3.1 Purity of the sample of b-tagged hemispheres

The purity P_b of the b-tagged sample of hemispheres is extracted from the data using a double-tagging technique, thereby minimising systematic uncertainties. The number of hemispheres N_t passing the b-flavour tagging criteria described above is counted together with the number of events N_{tt} where both hemispheres are b-tagged. With the b-tagging efficiencies for the b, c and light flavours given by η_b, η_c and η_{uds}, one can write

$$N_t = 2N_{MH}[R_b\eta_b + R_c\eta_c + (1 - R_b - R_c)\eta_{uds})], \quad (2)$$
$$N_{tt} = N_{MH}[C_b R_b \eta_b^2 + C_c R_c \eta_c^2$$
$$+ C_{uds}(1 - R_b - R_c)\eta_{uds}^2], \quad (3)$$

where N_{MH} represents the number of events that passed the multihadronic selection and fiducial cuts. R_b and R_c are the fractions of multihadronic Z^0 events decaying into

$b\bar{b}$ and $c\bar{c}$ pairs, respectively. The hemisphere correlation coefficients C_q, where q represents any primary quark flavour, are given by the ratio $C_q = \eta_{qq}/\eta_q^2$, where η_q is the efficiency for tagging a hemisphere containing flavour q and η_{qq} is the efficiency for tagging both hemispheres. Equations 2 and 3 can be re-expressed in terms of the purity P_b instead of η_b using the definition $P_b = 2N_{MH}R_b\eta_b$ $/N_t$, and then used to directly measure the b purity. Whilst the b purity can be determined from the direct solution of either Equation 2 or Equation 3 separately, the value of P_b is extracted by maximising the log-likelihood of both equations simultaneously to obtain the maximum statistical sensitivity.

A total of $N_{MH} = 2\,150\,423$ events passed the multihadronic event selection. These events contained $N_t = 303\,366$ b-tagged hemispheres, of which $N_{tt} = 45\,351$ have also the other hemisphere b-tagged. The world average values of R_b and R_c [3] are used as inputs. To extract P_b from Equations 2 and 3, the charm and light-flavour efficiencies η_c and η_{uds} and the correlation for b events, C_b, are taken from Monte Carlo, while C_c and C_{uds}, which have negligible impact on the b purity determination, are taken to be unity. From the fit to the data, the purity of all b-tagged hemispheres is measured to be $(91.901 \pm 0.016)\%$, where the error is statistical.

Extensive studies have been presented in a previous OPAL analysis on the systematic differences between data and Monte Carlo for C_b, η_c and η_{uds} [20]. Similar studies were conducted for this analysis. This was performed separately for the data collected in 1992 (19 % of the total data sample) where only $r - \phi$ information was available from the silicon microvertex detector, and for the larger part of the data, where z information was also available. The corresponding weighted averages for the combined sample are used as input parameters to the purity fit. The systematic uncertainties on P_b are summarised in Table 1. The purity is

$$P_b = (91.90 \pm 0.02\,(\text{stat.}) \pm 0.45\,(\text{syst.}))\% \quad (4)$$

for a b-tagging efficiency η_b of around 30 %.

Table 1. Contributions to the systematic uncertainty δP_b on the b purity P_b. For the input parameters taken from the Monte Carlo, the statistical and systematic uncertainties are shown separately. An error of 0.0000 indicates a value less than 0.00005

Input parameter	value	δP_b
R_c	0.177 ± 0.008	$\pm 0.19\%$
R_b	0.2169 ± 0.0012	$\pm 0.01\%$
η_c	0.0209 ± 0.0002 (MC stat.)	
	± 0.0014 (syst.)	$\pm 0.34\%$
η_{uds}	0.0034 ± 0.0000 (MC stat.)	
	± 0.0003 (syst.)	$\pm 0.22\%$
C_b	1.0493 ± 0.0052 (MC stat.)	
	± 0.0052 (syst.)	$\pm 0.01\%$
total		$\pm 0.45\%$

3.2 Electron identification

High-momentum electrons are searched for in the hemisphere opposite to a b-tagged hemisphere. Electrons are identified using an artificial neural network [20]. The six inputs used by this neural network are: the momentum and polar angle of the track; the ratio E/p of the electromagnetic energy and track momentum; the number of electromagnetic calorimeter blocks contributing to the energy measurement; the normalised ionization energy loss $dE/dx|_{norm}$ and its error. The normalised dE/dx value is defined as $dE/dx|_{norm} = (dE/dx - dE/dx|_0)/\sigma_0)$, where $dE/dx|_0$ is the ionization energy loss expected for an electron and σ_0 the error.

Candidate tracks must have a minimum of 40 jet chamber hits usable for the determination of the energy loss, out of a possible 159 hits. Electrons are required to have momentum greater than $2\,\mathrm{GeV}/c$. The momentum cut is applied to reduce the fraction of fake electrons and to restrict the analysis to the region where the input variables used for this neural network are properly modelled. Electrons from photon conversion and electrons from Dalitz decays are rejected as in [20].

In the data sample, 301 303 b-tagged hemispheres were selected when the sub-detectors required for electron identification were fully operational and 29 516 electrons were found in the opposite hemispheres. Monte Carlo events are used to determine the electron identification efficiency after b-tagging for $b \to e$ and $b \to c \to e$ decays. These are measured to be $\epsilon_{b\to e} = 0.5662 \pm 0.0012$ and $\epsilon_{b\to c\to e} = 0.3306 \pm 0.0012$, where the errors come from Monte Carlo statistics. The effect of the momentum cut at $2\,\mathrm{GeV}/c$ is taken into account.

3.3 Muon identification

All hemispheres opposite a b-tagged hemisphere are searched for muon candidates. Muons are identified by associating central detector tracks with track segments in the muon detectors in two orthogonal planes [22]. The muon candidates are also required to have momenta greater than $2\,\mathrm{GeV}/c$. In total, 44 832 muons are found in the hemispheres opposite 302 577 b-tagged hemispheres selected when the muon chambers were functional. The efficiencies for identifying muons in $b \to \mu$ and $b \to c \to \mu$ decays with momentum greater than $2\,\mathrm{GeV}/c$ are $\epsilon_{b\to\mu} = 0.6794 \pm 0.0011$ and $\epsilon_{b\to c\to\mu} = 0.4277 \pm 0.0013$, where the errors come from Monte Carlo statistics.

4 Composition of the lepton sample

The main contributions to the sample after selecting a lepton in a b-tagged event come from direct decays, $b \to \ell$, and cascade decays, $b \to c \to \ell$. All remaining sources are collectively referred to as background.

Fake muons form the largest source of background in the muon sample. These fake muons are mostly due

Table 2. Composition of the Monte Carlo sample of electron and muon candidates opposite a b-tagged hemisphere showing the contributions from $b \to \ell$, $b \to c \to \ell$ and background

Monte Carlo lepton candidates	104 653 e	173 735 μ
$b \to \ell$	54.7 %	43.0 %
$b \to c \to \ell$	27.1 %	23.0 %
fake leptons	3.3 %	18.5 %
non-prompt leptons	5.3 %	7.3 %
$b \to \bar{c} \to \ell$	3.5 %	3.1 %
$b \to \tau \to \ell$	2.5 %	1.8 %
$b \to J/\psi \to \ell^+\ell^-$	0.9 %	0.7 %
primary $c\bar{c}$ events	2.4 %	2.2 %
primary uds events	0.2 %	0.2 %
$g \to c\bar{c}$	0.2 %	0.1 %
$g \to b\bar{b}$	< 0.001 %	< 0.001 %

to light mesons passing through the hadronic calorimeter without showering. Fake electrons are less common and consist mostly of mis-identified pions. These fake leptons tend to have less transverse momentum than leptons from either $b \to \ell$ or $b \to c \to \ell$ decays. True leptons in $b\bar{b}$ events not originating from the semileptonic decay of a b or c quark, for example electrons from photon conversions, are grouped together as non-prompt leptons. The decays $b \to \bar{c} \to \ell$, where the $\bar{c}$ comes from the virtual W boson decay, form an important background to $b \to c \to \ell$ decays. The lepton coming from either of the two cascade decays tends to be produced with less transverse momentum with respect to the jet axis than a lepton coming from a direct $b \to \ell$ decay. The selected lepton samples also contain small contributions from $b \to \tau \to \ell$ and $b \to J/\psi \to \ell^+\ell^-$ decays. A smaller contribution to the backgrounds comes from leptons from charm and light flavour decays. Due to the high b purity of the selected data sample, this source is greatly suppressed. Finally, a very small contribution comes from gluon splitting into $c\bar{c}$ and $b\bar{b}$. The sources of background found in the Monte Carlo sample are shown in Table 2.

Instead of attempting to reject these backgrounds, a fit for the fractions of $b \to \ell$ and $b \to c \to \ell$ decays in the sample is performed using the two-dimensional distribution of the output variables of two neural networks: The first neural network, $NN_{b\ell}$, is trained to separate $b \to \ell$ events from all other events while the second, $NN_{bc\ell}$, is trained to separate $b \to c \to \ell$ events from all other events. Each of the neural networks is trained separately for electron and muon samples since the background is different in the two.

4.1 Neural network training

Jet and lepton kinematic variables in b-tagged events are used as input variables to train the neural networks $NN_{b\ell}$ and $NN_{bc\ell}$ to select direct and cascade leptons coming from b decays. By combining the information from several

variables, more discrimination power is obtained than by using momentum information alone. About 90 000 muon and 70 000 electron candidate tracks reconstructed in Monte Carlo events opposite a b-tagged hemisphere, were used to train $NN_{b\ell}$ and $NN_{bc\ell}$. Eight kinematic variables were used, which are shown in Fig. 1.

- lepton momentum;
- lepton p_T: the lepton transverse momentum calculated with respect to the nearest jet axis, excluding the lepton candidate itself;
- lepton jet energy: the energy of the jet containing the lepton;
- sub-jet energy: the energy of the sub-jet (defined below) containing the lepton;
- p_T sum: the scalar sum of transverse momenta of all charged tracks in the lepton jet;
- impact parameter: the impact parameter significance of the candidate lepton track with respect to the primary vertex;
- lepton Q_{jet}; the lepton charge multiplied by the jet charge (defined below) of the jet containing the lepton, including the lepton candidate track;
- opposite Q_{jet}: the lepton charge multiplied by the jet charge of the most energetic jet in the hemisphere opposite the lepton.

In $b \to \ell$ decays, the lepton momentum spectrum reflects the hard fragmentation of the primary b hadron and is thus efficient at separating these leptons from other sources. The boost along the b jet direction results in a higher lepton momentum for $b \to \ell$ than for other decays. Similarly, the decaying b hadron imparts more p_T to the lepton in $b \to \ell$ decays than in $b \to c \to \ell$ decays.

The total energy of the jet has sensitivity to leptons from direct decays since b jets are expected to have lower visible energy in semileptonic decays due to the emission of an energetic neutrino.

The smaller mass of c hadrons relative to b hadrons forces the non-leptonic decay products from a charm decay to follow the lepton direction more closely. The neutrino in a charm decay also carries less energy on average than the neutrino in a primary $b \to \ell$ decay. These differences mean that the energy deposited by neutral and charged particles in the vicinity of the lepton candidate, the lepton sub-jet energy, will be lower in $b \to \ell$ decays than in $b \to c \to \ell$ decays. The lepton jet is therefore divided into two sub-jets [23], where the initial sub-jet seeds are the lepton track and the other tracks in the jet. Each track and unassociated electromagnetic cluster is then reassigned iteratively until each one is closer in angle to its assigned sub-jet axis than to the other. No track or cluster is added to the sub-jet containing the lepton beyond an invariant mass upper limit of $2.5\,\mathrm{GeV/c^2}$. The "sub-jet energy" used for the neural network input refers to the sub-jet including the lepton.

The scalar sum of p_T for the jet characterises both the angular width and the multiplicity of the jet, both of which are known to differ significantly between b and charm and light-quark jets [24].
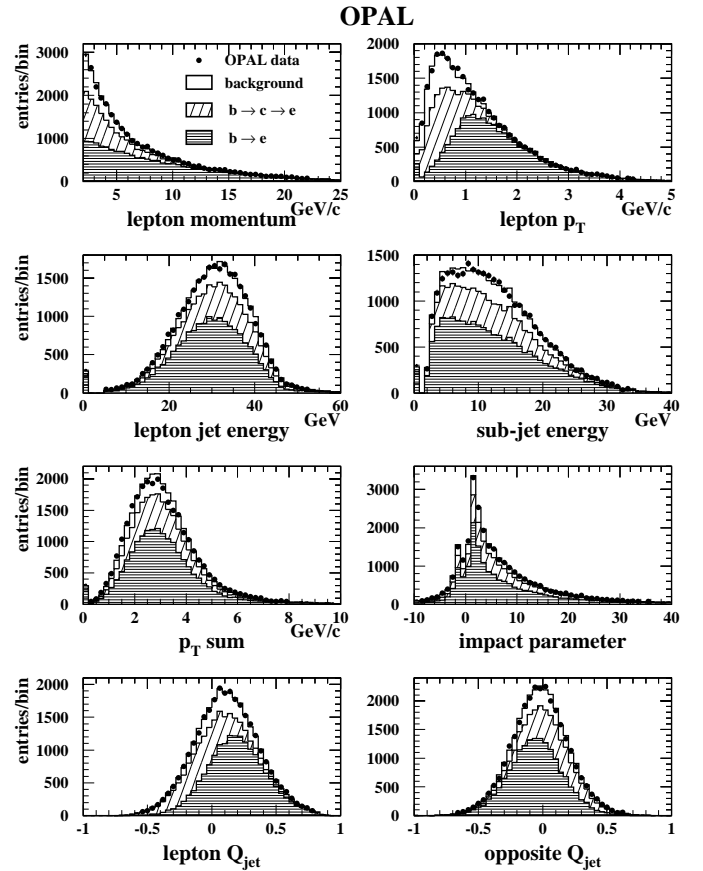

Fig. 1. The eight input variables used by the neural networks $NN_{b\ell}$ and $NN_{bc\ell}$ to separate $b \to \ell$ and $b \to c \to \ell$ decays. The contributions from the three classes of Monte Carlo events; $b \to \ell$, $b \to c \to \ell$ and backgrounds, are superimposed and compared to the data after normalisation and rescaling using the fractions $f(b \to \ell)$ and $f(b \to c \to \ell)$ derived in Sect. 5.2. The results are shown here for electrons only

The lepton impact parameter significance is the distance of closest approach of the track to the primary vertex divided by the uncertainty on this distance. Larger impact parameter significances are expected for leptons from decays such as $b \to \ell$ and $b \to c \to \ell$ decays, than for tracks from the primary vertex such as fragmentation tracks.

The final two variables consist of the reconstructed lepton charge multiplied by the jet charge for the jet associated with the lepton and for the most energetic jet in the b-tagged hemisphere. The jet charge is defined as

$$Q_{jet} = \frac{\sum\limits_{i} Q_i \cdot p_i^{0.5}}{\sum\limits_{i} p_i^{0.5}} \qquad (5)$$

where Q_i is the track charge, p_i is the track momentum and the sum runs over the charged tracks in the jet including the lepton candidate. Leptons from $b \to \ell$ decays have the same charge as the weakly decaying b quark and thus the lepton Q_{jet} variable shows a positive correlation
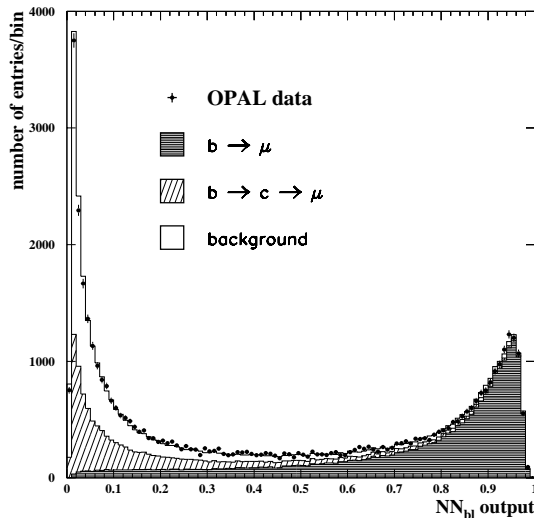
Fig. 2. Distribution of the output variable for the neural network $NN_{b\ell}$ trained specifically to distinguish $b \to \ell$ events from all other types of events. The three categories $b \to \ell$, $b \to c \to \ell$, and background are described in the text. The results are shown here for muons only
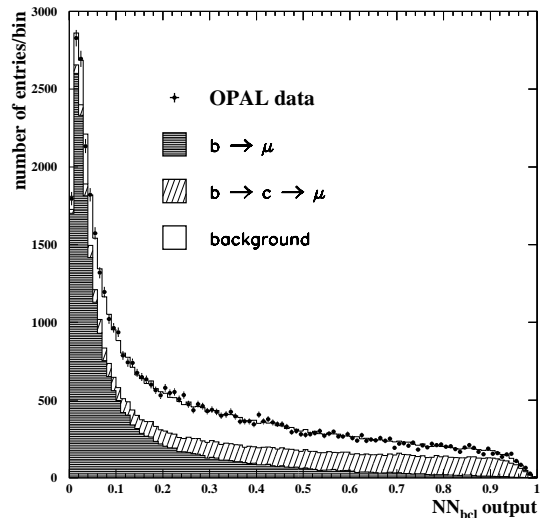
Fig. 3. Distribution of the output variable for the neural network $NN_{bc\ell}$ trained specifically to distinguish $b \to c \to \ell$ events from all other types of events. The three categories $b \to \ell$, $b \to c \to \ell$, and background are described in the text. The results are shown here for muons only

between the lepton charge and associated jet charge. Leptons from $b \to c \to \ell$ decays have opposite charge to the decaying b quark and hence show a negative correlation with the lepton jet charge. Leptons from $b \to \bar{c} \to \ell$ decays have a positive correlation with the lepton jet charge. In the absence of $B^0 - \overline{B^0}$ mixing, the correlations between the lepton charge in one hemisphere and the jet charge in the opposite hemisphere, embodied in the opposite Q_{jet} variable, are opposite to those of the jet associated with the lepton.

The distributions of the eight input variables used by the neural networks are shown for electrons in Fig. 1. The same good agreement between data and Monte Carlo simulation is found for muons for all input variables. Combining the information from these variables using neural networks allows not only to increase the separation power but also to include the correlations between the input variables.

The distribution of the neural network outputs from $NN_{b\ell}$ and $NN_{bc\ell}$ for muons are shown in Figs. 2 and 3. The results are shown for the three categories of Monte Carlo events: direct b decays $b \to \ell$, cascade decays $b \to c \to \ell$, and the background. As an indicator of the goodness-of-fit, the χ^2/bin is 1.00 in Fig. 2 and 0.88 in Fig. 3 and is calculated using the statistical, systematic and modelling errors (see Sect. 6).

As can be seen from Fig. 2, the neural network $NN_{b\ell}$ gives good separation of $b \to \ell$ decays from all other types of decays found in the b-tagged sample; there is much less separation power between $b \to c \to \ell$ events and the background. The second neural network, $NN_{bc\ell}$, gives further discrimination between $b \to c \to \ell$ events and all other events as can be seen in Fig. 3.

5 Calculation of the semileptonic branching ratios

The semileptonic branching fraction is given by

$$\text{BR}(b \to \ell X) = \frac{N_{b \to \ell}}{N_b} = \frac{N_\ell \cdot f(b \to \ell)}{\epsilon_{b \to \ell}} \cdot \frac{1}{N_{b-\text{tags}} \cdot P_b} \quad (6)$$

where $N_{b \to \ell}$ is the number of hemispheres containing a semileptonic b decay and N_b the total number of true b hemispheres. The fraction of $b \to \ell$ events determined by the fit, $f(b \to \ell)$, times the number of lepton candidates, N_ℓ, yields the number of $b \to \ell$ decays in the selected lepton sample. The total number of b events that decayed semileptonically, $N_{b \to \ell}$, is then obtained by correcting this number to account for the lepton detection efficiency, $\epsilon_{b \to \ell}$. The number of true b decays in the b-tagged sample, N_b, is obtained from the total number of b-tagged hemispheres, $N_{b-\text{tags}}$ scaled by the sample purity, P_b, as extracted from the data. This calculation is performed separately for electrons and muons. By replacing all occurrences of $b \to \ell$ by $b \to c \to \ell$ in Equation 6, one obtains the corresponding equation for $\text{BR}(b \to c \to \ell X)$.

5.1 Determining the lepton sample composition

The fractions of $b \to \ell$ and $b \to c \to \ell$ decays are extracted from the data by performing a binned log-likelihood fit to the data distributions of the neural network outputs using the shapes for each contribution obtained from the Monte Carlo. Two-dimensional distributions are formed using the neural network outputs $NN_{b\ell}$ and $NN_{bc\ell}$ with 20 by 20 bins. There are five fit parameters: the Peterson b fragmentation model parameter ϵ_b, $f(b \to e)$, $f(b \to \mu)$, $f(b \to c \to e)$ and $f(b \to c \to \mu)$. The remaining fraction

of selected candidates is assigned to the background sample: $b \to \bar{c} \to \ell$ leptons, non-prompt leptons and fake leptons in $b\bar{b}$ events, and leptons found in charm and light flavour events. Their fraction is fixed to be $1 - f(b \to \ell) - f(b \to c \to \ell)$ in the fit for electrons and muons separately. The Peterson b fragmentation model parameter ϵ_b is allowed to float in the fit, with a common value used for both electrons and muons, to greatly reduce the contributions to the systematic uncertainties from the modelling of this parameter. This is done by reweighting the Monte Carlo events such as to produce the desired fragmentation function.

5.2 Results

In total, 29 516 electrons and 44 832 muons are selected in the data opposite to a b-tagged hemisphere. The results of the fit are $f(b \to e) = 0.5726 \pm 0.0042$ and $f(b \to c \to e) = 0.2596 \pm 0.0055$ for electrons and $f(b \to \mu) = 0.4620 \pm 0.0034$ and $f(b \to c \to \mu) = 0.2166 \pm 0.0051$ for muons where the uncertainties are statistical. The Peterson fragmentation parameter is determined to be $\epsilon_b = 0.00573 \pm 0.00040(\text{stat.})$. These results include some small corrections described in the next section. Using these corrected parameters, the fit can adequately reproduce the observed distributions of the neural network output variables in data for all selected leptons, as shown above in Figs. 2 and 3.

The correlation coefficient between $f(b \to \ell)$ and $f(b \to c \to \ell)$ is -0.35 for electrons and -0.26 for muons. The correlations of $f(b \to e)$ and $f(b \to \mu)$ with the common fragmentation parameter are 0.32 and 0.39 respectively, whilst the fragmentation parameter produces a 0.13 correlation between $f(b \to e)$ and $f(b \to \mu)$. The size of all other correlations is below 0.06.

From Equation 6 using the b purity P_b as determined in Sect. 3.1, the semileptonic branching fractions are then determined to be

$$BR(b \to eX) = (10.78 \pm 0.08)\,\%,$$
$$BR(b \to \mu X) = (10.96 \pm 0.08)\,\%,$$
$$BR(b \to c \to eX) = (8.37 \pm 0.18)\,\%,$$
$$BR(b \to c \to \mu X) = (8.17 \pm 0.19)\,\%,$$

where the errors are statistical.

6 Systematic and modelling uncertainties

In this section, possible systematic shifts and uncertainties on the five fit parameters are estimated by studying detector modelling and experimental systematic effects on the results. The corresponding systematic uncertainties on $BR(b \to \ell X)$, $BR(b \to c \to \ell X)$ and $\langle x_E \rangle$ are compiled in Table 3.

6.1 Modelling the semileptonic decay lepton spectrum

Previous $BR(b \to \ell X)$ measurements [6–9] depended heavily on the proper modelling of the semileptonic decay spectrum. The exact shape of the lepton momentum spectrum is not known and little theoretical progress has been made in recent years. The use of neural networks to separate $b \to \ell$ and $b \to c \to \ell$ events from the background reduces the dependence of the branching ratio measurements on the shape of the lepton spectrum by making use of extra information such as jet shape and charge correlations. By taking into account all correlations, using more information and, most importantly, training two separate neural networks, the separation power is greatly enhanced, leading to reduced modelling errors. Nevertheless, the simulation of the b hadron decays and the prediction of the lepton momentum spectrum is still a large source of uncertainty.

Different decay models are used to estimate the effects of the modelling on the fitted fractions. The events are reweighted to reproduce the lepton momentum spectrum in the rest frame of the b hadron as predicted by the different models. The ACCMM model [14] predictions are used for $b \to \ell$ and $b \to c \to \ell$ decays to calculate the central values of $BR(b \to \ell X)$ and $BR(b \to c \to \ell X)$, using the prescription in [16]. The ISGW [25] and ISGW** models[2] provide the $\pm 1\sigma$ deviations for the $b \to \ell$ decays [16]. Although these models were derived using only B^0 and $B^\pm$ mesons, all b hadrons are reweighted. This has a very small effect on the central value but gives a more conservative estimate of the uncertainty on the modelling error than when only the B^0 and $B^\pm$ decays are reweighted. The agreement between the data and these and other semileptonic decay models is further investigated in the Appendix.

For the cascade decays, $b \to c \to \ell$, we use variations based on the CLEO measurements of the $b \to D$ spectrum combined with the ACCMM prediction for $c \to \ell$ decays as described in [16]. Since the b-tagging requirement highly suppresses contributions from charm and light flavours, the error from the semileptonic decay modelling in charm events is negligible, and these are simply reweighted to the central ACCMM model as described in [16]. Helicity effects in D^* decays are not taken into account but are expected to be very small.

Because of the minimum momentum cut of $2\,\text{GeV}/c$ imposed on the selected leptons, the measured lepton identification efficiencies correspond to a restricted momentum range. The effect of the extrapolation below the minimum momentum cut-off is taken into account when evaluating the lepton selection efficiency corresponding to the different models.

---

[2] This corresponds to a modification of the ISGW model introduced by the CLEO collaboration whereby all P-wave contributions (the D^{**} contributions) are increased from the nominal 11 % derived in the original model to 32 % to better describe their data.

6.2 Fragmentation models

Several models have been proposed to describe the heavy quark fragmentation process. The function of Peterson et al. [13] was used to simulate fragmentation in $b\bar{b}$ and $c\bar{c}$ events in the Monte Carlo. For b hadrons, the Peterson parameter is determined from the fit by reweighting the Monte Carlo events. For c hadrons, the parameter is varied between 0.025 to 0.031 to obtain a $\langle x_E \rangle$ for charm hadrons of 0.484 ± 0.008 [16]. As suggested in [16], the models of Collins and Spiller [26], and Kartvelishvili et al. [27] are used to estimate the systematic uncertainties coming from the shape of the b quark fragmentation function, quoted as the $+1\sigma$ and -1σ errors respectively. These models also have one free parameter. The Monte Carlo is reweighted to simulate each function and the free parameter as determined from the fit. The effects of the differing fragmentation functions and fitted parameters on the lepton efficiencies are also included in the fragmentation modelling error. The systematic uncertainties associated with the b fragmentation models are determined from the observed variations in the derived values of branching fractions obtained with the various functions. The agreement between the data and these functions is further discussed in the Appendix.

6.3 Lepton detection efficiencies

The electron detection efficiencies in data and Monte Carlo are compared for two pure electron samples: a low-momentum electron sample coming from photon conversions, and a high-momentum electron sample from Bhabha events. From these comparisons and from studying the neural network input variable distributions, a systematic uncertainty on the electron detection efficiency of 4 %, and an uncertainty on photon conversion rejection of 0.8 % is obtained [20].

The muon detection efficiency in data and Monte Carlo are compared for two samples: muon pairs from two-photon interactions and muons from $Z^0 \to \mu^+\mu^-$ decays. The first sample yields muons in the momentum range of 2 to 6 GeV/c, while the second sample gives muons with momentum greater than 30 GeV/c. In the data, 57 % of the selected muon sample is found in the lower range while only 0.2 % has momentum above 30 GeV/c. By comparing the selected muon samples, the Monte Carlo was found to slightly underestimate the efficiency in the data and so a multiplicative correction factor of 1.013 is applied to the measured efficiencies. A systematic uncertainty of 1.9 % is assigned to the muon detection efficiencies.

The systematic uncertainty associated with the momentum extrapolation below 2 GeV/c is discussed in Sect. 6.1.

6.4 Detector resolution effects

The tracking resolution and reconstruction efficiency could be slightly different for data and Monte Carlo. The reconstructed track parameters are smeared by ± 10 % in the Monte Carlo and the lepton detection efficiencies and the fit fractions recalculated. The difference from the final values for BR(b $\to \ell$X), BR(b $\to$ c $\to \ell$X) and the b fragmentation parameter are used as estimate of this source of systematic uncertainty.

6.5 Fake lepton rates

To study the fake rate in the muon sample, three different samples are used: identified pions in $K_s^0 \to \pi^+\pi^-$ decays, three prong τ decays, and a kaon enriched sample based on dE/dx requirements. From a comparison of the fake muon rates in data and Monte Carlo for these samples, it was determined that a correction factor of 1.11 ± 0.12 must be applied to the Monte Carlo events. Accordingly, the relative fraction of fake muon events is changed by $+11$ % using a reweighting technique. The weights are varied by ± 12 % and the data refitted. For electrons, studies on the fake rates were conducted using samples of photon conversion electrons and Bhabha events [20]. The fake rates measured in the data and Monte Carlo were consistent, such that no correction was required, but an uncertainty of ± 21 % is assigned for the fake electron rate.

6.6 b tagging purity

The systematic uncertainty on the value of the b purity obtained from the data is discussed in Sect. 3.1. This constitutes a 0.49 % relative error on the final values for BR(b $\to \ell$X) and BR(b $\to$ c $\to \ell$X). The errors on the b purity given in Table 1 have been further subdivided in Table 3 to show separately the contributions from uncertainties in R_c, R_b, $\langle x_E \rangle_c$ (the mean fraction of the beam energy carried by the weakly decaying charmed hadrons), gluon splitting to $b\bar{b}$ and $c\bar{c}$ pairs, the branching fraction of charmed mesons into K_s^0, charmed mesons lifetimes, decay multiplicities of charmed mesons and charm production fractions. The errors resulting from the uncertainty in the b purity due to detector resolution and finite Monte Carlo statistics are combined with the other contributions from these sources of error.

6.7 Modelling of the neural network input variables

Proper simulation of the lepton total and transverse momentum has already been addressed in Sects. 6.1 and 6.2. In addition, the effects of possible differences between the data and the Monte Carlo simulation of the other six variables used as inputs to the neural networks have been checked using the distributions given in Fig. 1. A qualitative check is obtained by verifying that the differences observed for each of these six variables is within the errors already assigned. No significant deviation is found. Nevertheless, the Monte Carlo distributions of these six variables are corrected by the observed difference between data and Monte Carlo to assign an error from this source. This is done for each variable by comparing the mean of

Table 3. Summary of all model-dependent and experimental systematic uncertainties on BR(b → ℓX) and BR(b → c → ℓX) (shown separately for electrons and muons), and $\langle x_E \rangle$. All errors are absolute errors given in percent (except for $\langle x_E \rangle$). The sign on each contribution indicates the correlation between this systematic uncertainty and the final results

Parameter	BR(b → e)	BR(b → c → e)	BR(b → μ)	BR(b → c → μ)	$\langle x_E \rangle$
		model-dependent sources			
b → ℓ	$^{-0.078}_{+0.207}$	$^{+0.126}_{-0.211}$	$^{-0.101}_{+0.221}$	$^{+0.206}_{-0.320}$	$^{-0.0051}_{+0.0081}$
b → c → ℓ	$^{-0.072}_{+0.057}$	$^{+0.149}_{-0.059}$	$^{-0.064}_{+0.058}$	$^{+0.168}_{-0.048}$	$^{+0.0009}_{-0.0008}$
fragmentation	$^{+0.047}_{-0.028}$	$^{+0.225}_{-0.144}$	$^{+0.096}_{-0.070}$	$^{+0.236}_{-0.180}$	$^{-0.0118}_{+0.0102}$
total models	$^{+0.220}_{-0.110}$	$^{+0.298}_{-0.262}$	$^{+0.248}_{-0.139}$	$^{+0.355}_{-0.370}$	$^{+0.0131}_{-0.0129}$
		systematic sources			
lepton efficiencies	∓0.440	∓0.341	∓0.208	∓0.155	
detector	±0.074	±0.113	±0.055	±0.086	±0.0004
lepton fake rates	±0.006	∓0.048	±0.037	∓0.106	∓0.0003
P_b : R_c	±0.022	±0.017	±0.022	±0.017	
R_b	∓0.001	∓0.001	∓0.001	∓0.001	
$\langle x_E \rangle_c$	±0.004	±0.003	±0.004	±0.003	
g→ b$\bar{\text{b}}$	±0.016	±0.013	±0.016	±0.013	
g→ c$\bar{\text{c}}$	±0.010	±0.008	±0.010	±0.008	
BR(D→ K_s^0)	±0.011	±0.008	±0.011	±0.008	
D^0 lifetime	±0.002	±0.002	±0.002	±0.002	
$D^{\pm}$ lifetime	±0.003	±0.002	±0.003	±0.002	
D_s lifetime	±0.001	±0.001	±0.001	±0.001	
D charged mult.	±0.011	±0.008	±0.011	±0.008	
D neutral mult.	∓0.024	∓0.018	∓0.024	∓0.018	
$f(c \to D^{\pm},\ D^0)$	±0.017	±0.014	±0.017	±0.014	
$f(c \to D_s)$	±0.002	±0.001	±0.002	±0.001	
$f(c \to \Lambda_c)$	∓0.007	∓0.005	∓0.007	∓0.005	
other NN inputs	±0.013	±0.090	±0.020	±0.129	±0.0001
MC statistics	±0.019	±0.042	±0.022	±0.049	±0.0010
b hadron species	∓0.013	±0.022	∓0.012	±0.030	∓0.0006
b → $X_u \ell \nu$	±0.004		±0.009	±0.022	∓0.0020
B mixing	±0.002	±0.016	∓0.002	±0.007	±0.0002
fake lepton spectrum		∓0.003	∓0.002	∓0.042	
b → τ → ℓ	∓0.026	∓0.013	∓0.021	∓0.019	±0.0003
b → $\bar{\text{c}}$ → ℓ	∓0.004	∓0.081	∓0.023	∓0.064	±0.0003
J/ψ → $\ell^+ \ell^-$	∓0.004		∓0.002		±0.0001
Λ_b polarisation	±0.004	±0.006	±0.005	±0.026	$^{-0.0013}_{+0.0020}$
experimental systematic	±0.450	±0.388	±0.228	±0.267	$^{+0.0031}_{-0.0027}$

the distribution in data with the mean of the sum of the three distributions (b → ℓ, b → c → ℓ and background) for the Monte Carlo. As expected, due to their smaller discrimination power, the changes observed on the fit results are very small and proportional to the discriminating power of the variable studied. The quadratic sum of the changes observed for the six input variables is used to assess the contribution from this source to the systematic uncertainty and is shown in Table 3.

6.8 Other sources of systematic uncertainties

Several other sources of systematic uncertainties have been investigated. The Monte Carlo is reweighted to simulate the desired parameters and the fit is repeated to assess the contributions to the systematic uncertainty. These sources are summarised in Table 3. Since their effects on the branching ratios and $\langle x_E \rangle$ are small, they are only described briefly here.

Finite Monte Carlo sample size: This includes contributions from the evaluation of η_c, η_{uds} and C_b from Table 1.

Table 4. Results for the data sample including all systematic uncertainties for electrons and muons. The uncertainties from detector resolution have been added to the errors on the fitted fractions $f(b \to \ell)$ and $f(b \to c \to \ell)$. The uncertainties due to semileptonic decay and fragmentation modelling are shown in the last error on the branching fractions

	electrons	muons
P_b	0.9190 ± 0.0002 (stat.) ± 0.0045 (syst.)	
N_{b-tags}	301303	302577
N_ℓ	29516	44832
$\epsilon_{b\to\ell}$	0.5662 ± 0.0231 (syst.)	0.6794 ± 0.0129 (syst.)
$f(b \to \ell)$	$0.5726 \pm 0.0042 \pm 0.0041$ (syst.)	$0.4620 \pm 0.0034 \pm 0.0031$ (syst.)
BR$(b \to \ell X)$	$(10.780 \pm 0.079 \pm 0.450\ ^{+0.220}_{-0.109})\,\%$	$(10.964 \pm 0.081 \pm 0.228\ ^{+0.248}_{-0.139})\,\%$
$\epsilon_{b\to c\to\ell}$	0.3306 ± 0.0135 (syst.)	0.4277 ± 0.0081 (syst.)
$f(b \to c \to \ell)$	$0.2596 \pm 0.0055 \pm 0.0047$ (syst.)	$0.2166 \pm 0.0051 \pm 0.0045$ (syst.)
BR$(b \to c \to \ell X)$	$(8.370 \pm 0.177 \pm 0.388\ ^{+0.298}_{-0.262})\,\%$	$(8.167 \pm 0.192 \pm 0.267\ ^{+0.355}_{-0.370})\,\%$

b hadron species: The production fraction for Λ_b baryons[3] is set to $(10.1\ ^{+3.9}_{-3.1})\,\%$ [3] and the semileptonic branching fraction for inclusive Λ_b is taken to be $(7.4 \pm 1.1)\,\%$ [4,28].

b $\to X_u \ell \nu$ transitions: The $b \to X_u \ell \nu$ branching fraction is set to $(1.84 \pm 0.79) \times 10^{-3}$, the combined value of [29].

$B^0 - \overline{B^0}$ mixing: The $B^0_d - \overline{B^0_d}$ mixing parameter is set to $\chi_d = 0.172 \pm 0.010$ [3] whilst 50% $B^0_s - \overline{B^0_s}$ mixing is assumed [3].

Fake lepton spectrum: Small variations in the distributions of fake leptons are allowed by shifting the momentum spectrum of fake leptons and non-prompt lepton in $b\bar{b}$ events by $25\,\mathrm{MeV}/c$, roughly $\pm 0.5\,\%$ of the mean momentum for fake and non-prompt leptons in $b\bar{b}$ events.

Contributions from b $\to \tau \to \ell$: The $b \to \tau \to \ell$ branching fractions are set to $(0.463 \pm 0.071)\,\%$ and $(0.452 \pm 0.069)\,\%$ [3] for electrons and muons, respectively.

Contributions from b $\to \bar{c} \to \ell$: This branching fraction is set to $(1.62\ ^{+0.44}_{-0.36})\,\%$ as derived in [30].

Contributions from b $\to J/\psi \to \ell^+ \ell^-$: The experimental value given in [3] for BR$(b \to J/\psi)$ is $(1.16 \pm 0.10)\,\%$. Combined with a recent BES measurement for BR$(J/\psi \to \ell^+ \ell^-) = (5.87 \pm 0.10)\,\%$ [31], this gives BR$(b \to J/\psi \to \ell^+ \ell^-) = (0.0681 \pm 0.0060)\,\%$.

Effect of Λ_b polarisation: Leptons coming from semileptonic Λ_b decays are reweighted to simulate a spectrum corresponding to -56% polarisation according to [32]. The systematic errors are calculated using the polarisation range -13% to -87%, the 95% confidence level limits from [32].

Bias from the opposite jet charge variable: To check that no bias is introduced by using the jet charge from the opposite side (the b-tagged hemisphere), a test is made in which this information is removed from the neural network. The central values returned by the fit changed by

much less than one standard deviation. Hence, no correction is deemed necessary.

6.9 Consistency checks

To test the fitting procedure, the Monte Carlo sample is divided into two equal sub-samples. The first sample is used as a substitute for the real data in the fit while the second is retained as the Monte Carlo sample. The fitted fractions for the first sample can then be compared to the true information from the Monte Carlo. The fitted fractions and the Peterson fragmentation parameter all agree with the true values within statistics.

Various tests are performed on the data to check the stability of the results by varying the selection criteria. Firstly, the effect of changing the minimum lepton momentum requirement on the measured value for BR$(b \to \ell X)$ is investigated. The minimum lepton momentum cut is increased from the nominal $2.0\,\mathrm{GeV}/c$ to $5.0\,\mathrm{GeV}/c$ in steps of $0.5\,\mathrm{GeV}/c$ and BR$(b \to \ell X)$ is recalculated each time. This test was found to yield good agreement when performed using the Monte Carlo test samples discussed above. Similarly, a cut is applied on the neural network $NN_{b\ell}$ output variable shown in Fig. 2. The cut is increased by steps of 0.1 from 0.0 to 0.6. A similar test is performed to check the stability of the BR$(b \to c \to \ell X)$ results by imposing a cut on the neural network $NN_{bc\ell}$ output variable shown in Fig. 3. The cut is increased up to a value of 0.4. For all these tests, the variations observed are found to be statistically consistent with the central values calculated for BR$(b \to \ell X)$ and BR$(b \to c \to \ell X)$.
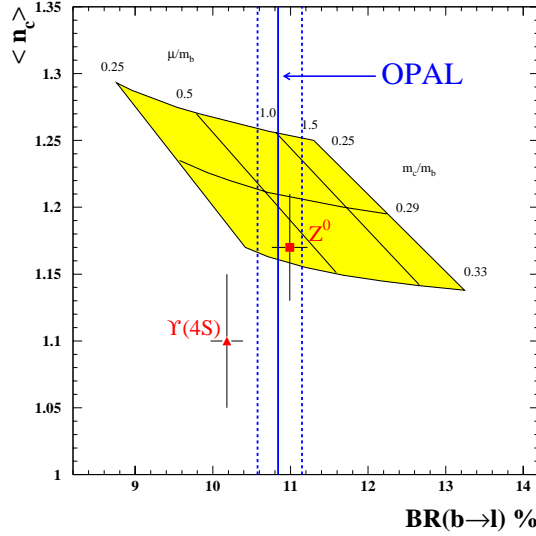
Varying the binning used to perform the fit has no significant influence on the central values for BR$(b \to \ell X)$ and BR$(b \to c \to \ell X)$. The central results are derived using 20 by 20 bins for the 2-dimensional fit to $NN_{b\ell}$ and $NN_{bc\ell}$. This range is varied from 5 by 5 up to 40 by 40 bins, yielding consistent values for the branching fractions.

Lastly, the data are divided into four sub-samples corresponding to the different years in which the data were taken. The b-tagging purity is recalculated for each data

---

[3] Λ_b denotes all weakly-decaying b baryons produced in Z^0 decays

Table 5. The full systematic correlation matrix from the averaging procedure of BR(b $\to$ eX), BR(b $\to$ μX), BR(b $\to$ c $\to$ eX) and BR(b $\to$ c $\to$ μX)

	BR(b $\to$ eX)	BR(b $\to$ c $\to$ eX)	BR(b $\to$ μX)	BR(b $\to$ c $\to$ μX)
BR(b $\to$ eX)	1.00			
BR(b $\to$ c $\to$ eX)	0.40	1.00		
BR(b $\to$ μX)	0.34	-0.21	1.00	
BR(b $\to$ c $\to$ μX)	-0.25	0.50	-0.21	1.00

Fig. 4. The number of charm hadrons per b hadron decay, $\langle n_c \rangle$, as a function of BR(b $\to$ ℓX) for the Z^0 [3] and BR(B $\to$ Xℓ) for the Υ(4S) result [3]. The result derived in this analysis is superimposed as a vertical line with error bars. The shaded box represents the theoretical calculation in the framework of Heavy Quark Effective Theory including higher-order corrections as given in [2] for different assumptions for the ratio of the renormalisation scale μ and the b quark mass m_b, and the ratio of the c and b quark masses, m_c/m_b. A correction of τ_b/τ_B has been applied to the theoretical prediction and to the Υ(4S) result, as described in the text

sub-set separately. Taking the uncorrelated systematic errors into account, all sub-samples are found to be statistically consistent with the full data sample.

7 Results and conclusions

All the relevant quantities needed to calculate the branching ratios BR(b $\to$ ℓX) and
BR(b $\to$ c $\to$ ℓX) are given in Table 4. The values

$$\mathrm{BR}(\mathrm{b} \to e\mathrm{X}) = (10.78 \pm 0.08 \ (\text{stat.})$$
$$\pm 0.45 \ (\text{syst.}) \ ^{+0.22}_{-0.11} \ (\text{model}))\,\%$$
$$\mathrm{BR}(\mathrm{b} \to \mu\mathrm{X}) = (10.96 \pm 0.08 \ (\text{stat.})$$
$$\pm 0.23 \ (\text{syst.}) \ ^{+0.25}_{-0.14} \ (\text{model}))\,\%$$
$$\mathrm{BR}(\mathrm{b} \to \mathrm{c} \to e\mathrm{X}) = (8.37 \pm 0.18 \ (\text{stat.})$$
$$\pm 0.39 \ (\text{syst.}) \ ^{+0.30}_{-0.26} \ (\text{model}))\,\%$$

$$\mathrm{BR}(\mathrm{b} \to \mathrm{c} \to \mu\mathrm{X}) = (8.17 \pm 0.19 \ (\text{stat.})$$
$$\pm 0.27 \ (\text{syst.}) \ ^{+0.36}_{-0.37} \ (\text{model}))\,\%$$

are obtained for the semileptonic branching ratios for electrons and muons, consistent with lepton universality. These four branching ratios are combined together to obtain

$$\mathrm{BR}(\mathrm{b} \to \ell\mathrm{X}) = (10.84 \pm 0.09 \ (\text{stat.})$$
$$\pm 0.21 \ (\text{syst.}) \ ^{+0.21}_{-0.13} \ (\text{model}))\,\%$$
$$\mathrm{BR}(\mathrm{b} \to \mathrm{c} \to \ell\mathrm{X}) = (\ 8.39 \pm 0.15 \ (\text{stat.})$$
$$\pm 0.22 \ (\text{syst.}) \ ^{+0.33}_{-0.29} \ (\text{model}))\,\%.$$

taking into account the full covariance matrix as in [16]. The BR(b $\to$ ℓX) measurement is the most precise to date at the Z^0 resonance whereas BR(b $\to$ c $\to$ ℓX) is more precise than the current world average value of $(7.8 \pm 0.6)\%$ [3]. The value derived for BR(b $\to$ c $\to$ ℓX) is outside the range given by BR(b $\to$ c $\to$ eX) and BR(b $\to$ c $\to$ μX) due to large off-diagonal terms in the covariance matrix and strong correlations with the BR(b $\to$ ℓX) measurement. The statistical error on BR(b $\to$ ℓX) is larger than the individual errors on BR(b $\to$ eX) and BR(b $\to$ μX) since the statistical errors from BR(b $\to$ c $\to$ eX) and BR(b $\to$ c $\to$ μX) also contribute. The full systematic correlation matrix is given in Table 5.

The BR(b $\to$ eX) and BR(b $\to$ μX) measurements presented here are consistent with the current average of all Z^0 measurements, $\mathrm{BR}^b_{SL} = (10.99 \pm 0.23)\,\%$ [3], based on a global fit to several electroweak parameters and including specific measurements of BR(b $\to$ ℓX) [6–9]. On the other hand, the measurement of BR(b $\to$ ℓX) is still larger than the Υ(4S) measurement of $\mathrm{BR}^B_{SL} = (10.45 \pm 0.21)\,\%$ [3], when it is expected to be lower, as explained in Sect. 1. If the lifetime ratio correction is applied, the difference between this result and the Υ(4S) measurement is about 1.8 standard deviations.

This measurement is also consistent with theoretical calculations as can be seen in Fig. 4, where a correction factor of 0.974 corresponding to the lifetime ratio τ_b/τ_B [3] has been applied to both the theoretical calculations and the Υ(4S) value of BR(B $\to$ Xℓ) to allow direct comparison with the Z^0 results. No correction is applied to the values of $\langle n_c \rangle$, the average number of charm hadrons produced per b decay.

From the fitted fragmentation model parameters, the average value of the fraction of the beam energy carried

by the weakly decaying b hadron is obtained, giving

$$\langle x_E \rangle = 0.709 \pm 0.003 \text{ (stat.)}$$
$$\pm 0.003 \text{ (syst.)} \pm 0.013 \text{ (model)}$$

where the modelling error is dominated by the choice of b fragmentation model.

All the measurements presented here are statistically independent of, and consistent with similar results derived in a previous OPAL analysis [6] where the quantities BR(b → ℓX) = $(10.5 \pm 0.6 \text{ (stat.)} \pm 0.5 \text{ (syst.)}) \%$, BR(b → c → ℓX) = $(7.7 \pm 0.4 \pm 0.7) \%$ and $\langle x_E \rangle = 0.697 \pm 0.006 \text{ (stat.)} \pm 0.011 \text{ (syst.)}$ were extracted from a fit for these and several other parameters (including R_b). However, the uncertainties related to assessing the systematic correlations between these old results and those presented in this paper means that no overall gain in precision is obtained by combining them. Therefore the results presented here supersede the results previously published in [6].

Appendix

Semileptonic b decay and fragmentation models

For the first time at LEP, an attempt is made to probe the level of agreement between the data and various semileptonic decay models. This test is also sensitive enough to allow a closer examination of different fragmentation functions. In this section, several theoretical b → ℓ decay models are investigated. These models affect both the lepton total and transverse momentum spectra. For each b → ℓ decay model, we use three different fragmentation functions, those of Peterson et al. [13], Collins and Spiller [26] and Kartvelishvili et al. [27]. These functions primarily affect the lepton total momentum spectrum, leaving the transverse momentum unchanged. The same models are used to simulate the cascade decays b → c → ℓ, and to assess the modelling uncertainties, as described in Sect. 6.1.

The six b → ℓ decay models investigated are:

1. ACCMM model [14]: all parameters were tuned to the CLEO data [15]. Their values are fixed as given in [16]: the Fermi momentum of the spectator quark, $p_F = 298 \text{ MeV/c}$, the mass of the charm quark, $m_c = 1673 \text{ MeV/c}^2$, and the mass of the spectator quark, $m_{sp} = 150 \text{ MeV/c}^2$.

2. ISGW model [25]: this model has no free parameters and the D^{**} contributions are predicted to account for 11 % of all b decays.

3. ISGW** model: the ISGW model modified such as to allow the total contributions from D^{**} to account for 32 % of all b decays, as described in [16].

4. ISGW2 [33]: a revised version of the ISGW model incorporating constraints from heavy quark symmetry, hyperfine distortions of wave functions, and form factors with more realistic high-recoil behaviour. This model predicts that the sum of all D^{**} contributions accounts for 9.3 % of the total b decay width. The $b \to X_u \ell \nu$ branching ratio was fixed to 2.2 % of all b decays and mixing was assumed between the η and η' final states.

5. ISGW2**: the ISGW2 model modified to allow the sum of all D^{**} contributions to be a free parameter of the fit. Best agreement with OPAL data is found when the D^{**} contribution amounts to $(45 \pm 3 \text{ (stat.)} \pm 3 \text{ (syst.)} \pm 4 \text{ (model)}) \%$ of the total width, instead of the 9.3 % set in the original model. The model error contains uncertainties from both the b fragmentation (following the same procedure as described in Sect. 6.2) and b → c → ℓ decay models. The Peterson fragmentation model is used to derive the central value.

6. ACCMM*: the ACCMM model with free parameters. The Fermi momentum of the spectator quark, p_F, and the mass of the charm quark, m_c, are treated as free parameters in the fit, giving $p_F = (837 \pm 143 \text{ (stat.)} \pm 132 \text{ (syst.)} {}^{+234}_{-186} \text{ (model)}) \text{ MeV/c}$ and $m_c = (1287 \pm 100 \text{ (stat.)} \pm 87 \text{ (syst.)} {}^{+112}_{-136} \text{ (model)}) \text{ MeV/c}^2$. The mass of the spectator quark is kept fixed at 150 MeV/c^2 as in [16].

   The semileptonic decay model parameters p_F and m_c strongly depend on the choice of the fragmentation model used. The Peterson model is used to derive the central values. The modelling errors given here again correspond to the b fragmentation and b → c → ℓ decay model errors added in quadrature. The correlation coefficient between these model parameters is -0.970. The decay model parameters are consistent with the calculated p_F value of about 550 MeV/c derived in [34] using the relativistic quark model, and the world average charm mass of 1100 to 1400 MeV/c^2 taken from [3]. The $b \to X_u \ell \nu$ branching ratio was fixed to 2.7 % of all b decays.
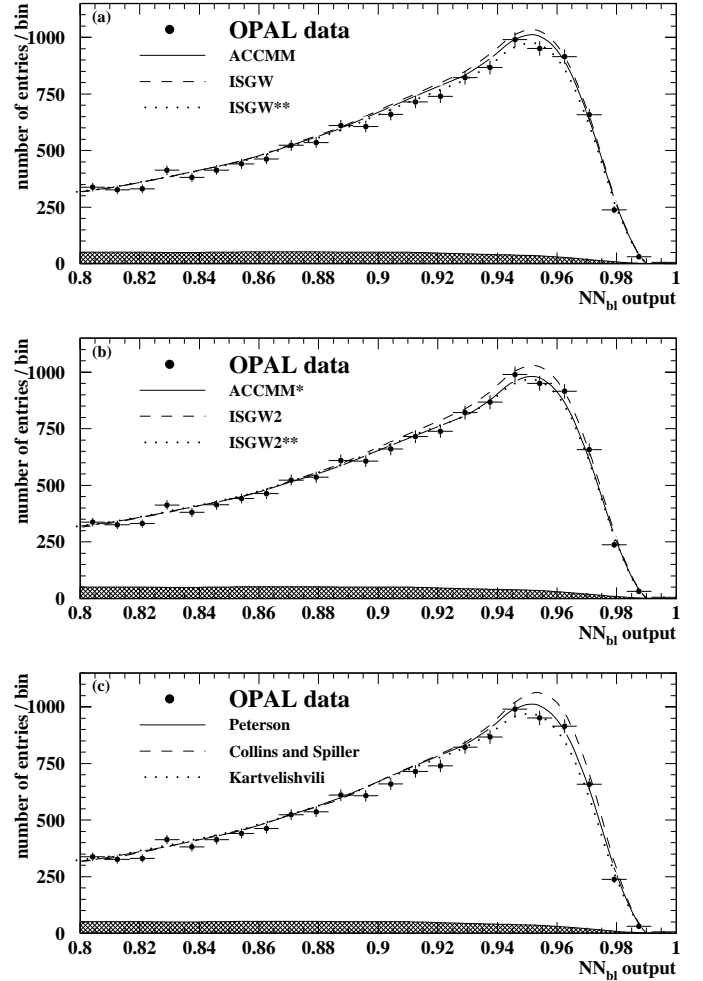
Figures 5 and 6 show the fitted distributions for each of these models compared to the data in the b → ℓ peak re-
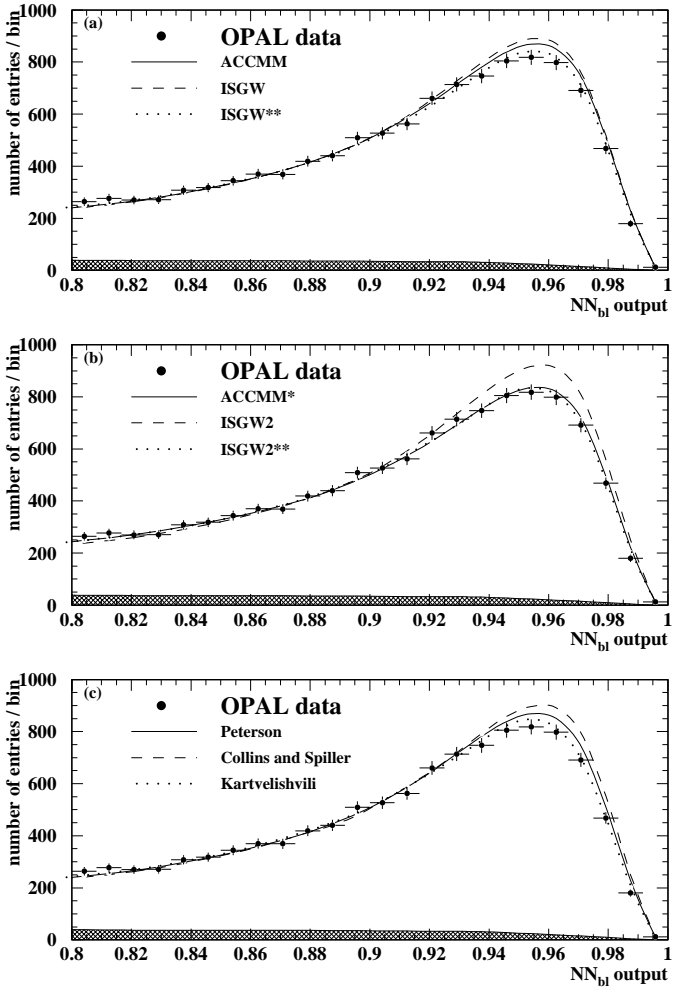
Fig. 5a–c. The fitted distributions for the $NN_{b\ell}$ neural network output for electrons with **a** the ACCMM, ISGW and ISGW** models; **b** the ISGW2, ISGW2** and ACCMM* models; **c** the ACCMM model with the Peterson, Collins and Spiller and Kartvelishvili fragmentation functions. The Peterson function is used to describe the fragmentation in **a** and **b**. The shaded area shows contributions from sources other than $b \to e$ in the data, as extracted from the fit

Fig. 6a–c. The fitted distributions for the $NN_{b\ell}$ neural network output for muons with **a** the ACCMM, ISGW and ISGW** models; **b** the ISGW2, ISGW2** and ACCMM* models; **c** the ACCMM model with the Peterson, Collins and Spiller and Kartvelishvili fragmentation functions. The Peterson function is used to describe the fragmentation in **a** and **b**. The shaded area shows contributions from sources other than $b \to \mu$ in the data, as extracted from the fit

gion of the $NN_{b\ell}$ neural network output distributions for electrons and muons, respectively. The fit is performed over the full range of the neural network output (from zero to one). The region shown corresponds to $NN_{b\ell} > 0.8$, which, from the fit results to the data, is approximately 93 % pure in $b \to \ell$ decays.

The results for $BR(b \to \ell X)$ and $BR(b \to c \to \ell X)$ obtained with these different models are summarised in Table 6 together with the statistical, systematic and modelling uncertainties. All errors are calculated according to the procedures outlined in the preceding sections, apart from the modelling error which accounts for $b \to c \to \ell$ decay modelling only. The values obtained for the decay model parameters as well as for the free parameter in the fragmentation functions are also given in Table 6. The results for $\langle x_E \rangle$ corresponding to the various fitted fragmentation functions are also listed. These can be compared to

the value of $\langle x_E \rangle = 0.702 \pm 0.008$ from [30] obtained from a multi-parameter fit to several electroweak parameters. The χ^2/bin is calculated using the portion of the $NN_{b\ell}$ output shown in Figs. 5 and 6 using statistical, systematic and modelling uncertainties from both the electron and muon samples. These are given as an indicator of the agreement between these models and the data.

The accuracy of the test does not allow ruling out specific $b \to \ell$ models, although some trends are clear:

– The fragmentation functions of Peterson et al. and Kartvelishvili et al. provide equally good fits to the data. The fragmentation function of Collins and Spiller is generally disfavoured by our data.
– The semileptonic decay models ISGW** and ISGW2** best agree with our data when used with the b fragmentation models of Peterson et al. or Kartvelishvili et al. However, these models are less theoretically sound

Table 6. Branching fractions BR(b → ℓX) and BR(b → c → ℓX) (given in %) derived by comparing the data to three fragmentation functions and various semileptonic decay models for b → ℓ decays. The uppermost line corresponds to the central results, as discussed in Sect. 7. The quoted errors on the branching ratios correspond to the statistical, systematic and b → ℓ modelling errors, respectively. The fitted b → ℓ decay model parameters are also given when appropriate. The fitted b fragmentation function parameters, and the corresponding values for $\langle x_E \rangle$ are presented. The combined statistical, systematic and b → c → ℓ modelling errors are given for all fitted model parameters. The χ^2/bin is calculated using the portion of the NN$_{b\ell}$ output shown in Figs. 5 and 6, using all uncertainties from both the electron and muon samples; these are given as an indicator of the goodness-of-fit. All models and their parameters are described in the text

b → ℓ model	b → ℓ model parameters	Fragmentation parameter	$\langle x_E \rangle$	BR(b → eX)	BR(b → μX)	BR(b → c → eX)	BR(b → c → μX)	χ^2/bin
Peterson et al.								
ACCMM	fixed	0.00573 ± 0.00062	0.709 ± 0.004	10.78 ± 0.08 ± 0.45 $^{-0.06}_{-0.07}$	10.96 ± 0.08 ± 0.23 $^{-0.06}_{-0.09}$	8.37 ± 0.18 ± 0.38 $^{+0.15}_{-0.06}$	8.17 ± 0.19 ± 0.23 $^{+0.17}_{-0.05}$	64/48
ISGW	fixed	0.00655 ± 0.00070	0.705 ± 0.004	10.70 ± 0.08 ± 0.45 $^{+0.09}_{-0.07}$	10.86 ± 0.08 ± 0.23 $^{+0.09}_{+0.07}$	8.50 ± 0.18 ± 0.38 $^{-0.06}_{-0.16}$	8.37 ± 0.19 ± 0.24 $^{-0.05}_{-0.16}$	98/48
ISGW**	fixed	0.00456 ± 0.00051	0.718 ± 0.004	10.99 ± 0.08 ± 0.46 $^{+0.06}_{-0.06}$	11.19 ± 0.08 ± 0.23 $^{+0.06}_{-0.06}$	8.16 ± 0.18 ± 0.37 $^{-0.06}_{-0.14}$	7.85 ± 0.20 ± 0.23 $^{-0.04}_{-0.19}$	37/48
ISGW2	fixed	0.00787 ± 0.00083	0.698 ± 0.004	10.69 ± 0.08 ± 0.45 $^{+0.06}_{-0.06}$	10.86 ± 0.08 ± 0.23 $^{+0.06}_{-0.06}$	8.62 ± 0.18 ± 0.38 $^{-0.06}_{-0.16}$	8.55 ± 0.19 ± 0.24 $^{-0.07}_{-0.15}$	131/48
ISGW2**	$f_{D^{**}} = 45 \pm 5$	0.00446 ± 0.00055	0.719 ± 0.004	10.95 ± 0.08 ± 0.45 $^{+0.06}_{-0.07}$	11.15 ± 0.08 ± 0.23 $^{+0.06}_{-0.09}$	8.17 ± 0.18 ± 0.37 $^{-0.06}_{-0.19}$	7.85 ± 0.20 ± 0.23 $^{-0.03}_{-0.40}$	35/48
ACCMM*	$p_F = 837\,^{+204}_{-217}$ $m_c = 1287\,^{+142}_{-135}$	0.00465 ± 0.00054	0.717 ± 0.004	10.95 ± 0.09 ± 0.46 $^{-0.11}_{+0.08}$	11.15 ± 0.09 ± 0.23 $^{-0.10}_{+0.08}$	8.16 ± 0.18 ± 0.37 $^{+0.23}_{-0.08}$	7.84 ± 0.20 ± 0.23 $^{+0.51}_{-0.09}$	38/48
Collins and Spiller								
ACCMM	fixed	0.00342 ± 0.00062	0.698 ± 0.004	10.83 ± 0.08 ± 0.45 $^{-0.07}_{-0.07}$	11.06 ± 0.08 ± 0.23 $^{-0.07}_{+0.06}$	8.60 ± 0.18 ± 0.38 $^{+0.15}_{-0.06}$	8.40 ± 0.19 ± 0.24 $^{+0.18}_{-0.06}$	148/48
ISGW	fixed	0.00421 ± 0.00074	0.693 ± 0.004	10.74 ± 0.08 ± 0.45 $^{+0.06}_{-0.07}$	10.95 ± 0.08 ± 0.23 $^{+0.06}_{+0.07}$	8.72 ± 0.18 ± 0.38 $^{-0.06}_{-0.16}$	8.61 ± 0.19 ± 0.24 $^{-0.06}_{-0.17}$	202/48
ISGW**	fixed	0.00241 ± 0.00044	0.705 ± 0.004	11.05 ± 0.08 ± 0.46 $^{+0.06}_{-0.06}$	11.30 ± 0.08 ± 0.23 $^{+0.06}_{-0.06}$	8.39 ± 0.18 ± 0.38 $^{-0.06}_{-0.14}$	8.09 ± 0.20 ± 0.23 $^{-0.05}_{-0.20}$	84/48
ISGW2	fixed	0.00556 ± 0.00096	0.687 ± 0.004	10.72 ± 0.08 ± 0.45 $^{+0.06}_{-0.07}$	10.94 ± 0.08 ± 0.23 $^{+0.07}_{-0.06}$	8.83 ± 0.18 ± 0.39 $^{-0.06}_{-0.16}$	8.79 ± 0.19 ± 0.24 $^{-0.08}_{-0.16}$	253/48
ISGW2**	$f_{D^{**}} = 43 \pm 5$	0.00251 ± 0.00044	0.704 ± 0.004	11.00 ± 0.08 ± 0.45 $^{+0.06}_{-0.07}$	11.24 ± 0.08 ± 0.23 $^{+0.08}_{-0.07}$	8.43 ± 0.18 ± 0.38 $^{-0.06}_{-0.19}$	8.14 ± 0.20 ± 0.23 $^{-0.04}_{-0.41}$	80/48
ACCMM*	$p_F = 679\,^{+180}_{-192}$ $m_c = 1287\,^{+146}_{-138}$	0.00252 ± 0.00043	0.704 ± 0.004	10.94 ± 0.09 ± 0.45 $^{-0.11}_{+0.08}$	11.19 ± 0.09 ± 0.23 $^{-0.10}_{+0.08}$	8.43 ± 0.18 ± 0.38 $^{+0.23}_{-0.08}$	8.14 ± 0.20 ± 0.23 $^{+0.49}_{-0.09}$	88/48
Kartvelishvili et al.								
ACCMM	fixed	10.04 ± 0.57	0.720 ± 0.005	10.75 ± 0.08 ± 0.45 $^{-0.07}_{-0.07}$	10.89 ± 0.08 ± 0.23 $^{-0.07}_{-0.06}$	8.23 ± 0.18 ± 0.37 $^{+0.15}_{-0.06}$	7.99 ± 0.19 ± 0.23 $^{+0.16}_{-0.04}$	41/48
ISGW	fixed	9.40 ± 0.54	0.714 ± 0.005	10.69 ± 0.08 ± 0.45 $^{+0.06}_{-0.07}$	10.80 ± 0.08 ± 0.23 $^{+0.06}_{-0.07}$	8.36 ± 0.18 ± 0.37 $^{-0.06}_{-0.16}$	8.20 ± 0.19 ± 0.24 $^{-0.04}_{-0.15}$	56/48
ISGW**	fixed	11.23 ± 0.63	0.729 ± 0.005	10.94 ± 0.08 ± 0.45 $^{+0.06}_{-0.07}$	11.10 ± 0.08 ± 0.23 $^{+0.06}_{-0.07}$	8.01 ± 0.18 ± 0.37 $^{-0.06}_{-0.14}$	7.66 ± 0.20 ± 0.22 $^{-0.03}_{-0.18}$	48/48
ISGW2	fixed	8.58 ± 0.49	0.706 ± 0.005	10.69 ± 0.08 ± 0.45 $^{+0.06}_{-0.07}$	10.81 ± 0.08 ± 0.23 $^{+0.06}_{-0.07}$	8.48 ± 0.18 ± 0.38 $^{-0.06}_{-0.16}$	8.39 ± 0.19 ± 0.24 $^{-0.06}_{-0.14}$	73/48
ISGW2**	$f_{D^{**}} = 46 \pm 5$	11.44 ± 0.67	0.731 ± 0.005	10.91 ± 0.08 ± 0.45 $^{+0.06}_{-0.07}$	11.07 ± 0.08 ± 0.23 $^{+0.06}_{-0.06}$	8.01 ± 0.18 ± 0.37 $^{-0.06}_{-0.19}$	7.65 ± 0.20 ± 0.22 $^{-0.02}_{-0.39}$	53/48
ACCMM*	$p_F = 1063\,^{+409}_{-368}$ $m_c = 1153\,^{+184}_{-199}$	10.96 ± 0.64	0.727 ± 0.005	10.95 ± 0.09 ± 0.46 $^{-0.11}_{+0.11}$	11.11 ± 0.10 ± 0.23 $^{-0.10}_{+0.11}$	8.00 ± 0.18 ± 0.37 $^{+0.23}_{-0.10}$	7.64 ± 0.20 ± 0.22 $^{+0.52}_{-0.20}$	39/48

since modifications to the original models were needed to allow the overall fraction of D** contributions to be a free fit parameter when this fraction is in fact one of the predictions of the models.

– For the ACCMM* semileptonic decay model, the best fit to the data is obtained with

$$p_F =$$
$$(837 \pm 143 \,(\text{stat.}) \pm 132 \,(\text{syst.}) \,^{+234}_{-186} \,(\text{model})) \,\text{MeV/c},$$
$$m_c =$$
$$(1287 \pm 100 \,(\text{stat.}) \pm 87 \,(\text{syst.}) \,^{+112}_{-136} \,(\text{model})) \,\text{MeV/c}^2$$

when the mass of the spectator quark is kept fixed at $150 \,\text{MeV/c}^2$. These results are derived using the b fragmentation model of Peterson et al.

– The ISGW2 model gives a worse agreement with our data than the ISGW model, with all fragmentation models.

References

1. E. Bagan, P. Ball, V.M. Braun, and P. Gosdzinsky, *Nucl. Phys.* B**432** (1994) 3 and *Phys. Lett.* B**342** (1995) 362; E. Bagan, P. Ball, B. Fiol, and P. Gosdzinsky, *Phys. Lett.* B**351** (1995) 546
2. M. Neubert, C.T. Sachrajda, *Nucl. Phys.* B**483** (1997) 339
3. Review of Particle Physics, C. Caso et al. (Particle Data Group), *Eur. Phys. J.* C**3** (1998) 1
4. OPAL Collab., R. Akers et al., *Z. Phys.* C**74** (1997) 423
5. Production and decay of b-flavoured hadrons, K. Honscheid, *Eur. Phys. J.* C**3** (1998) 522
6. OPAL Collab., R. Akers et al., *Z. Phys.* C**60** (1993) 199
7. ALEPH Collab., D. Buskulic et al., *Phys. Lett.* B**384** (1996) 414; ALEPH Collab., D. Buskulic et al., *Z. Phys.* C**62** (1994) 179
8. DELPHI Collab., P. Abreu et al., *Z. Phys.* C**66** (1995) 323
9. L3 Collab., M. Acciarri et al., *Z. Phys.* C**71** (1996) 379; L3 Collab., M. Acciarri et al., *Phys. Lett.* B**335** (1994) 542; L3 Collab., O. Adriani et al., *Phys. Lett.* B**292** (1992) 454
10. OPAL Collab., K. Ahmet et al., *Nucl. Instr. and Meth.* A**305** (1991) 275; P.P. Allport et al., *Nucl. Instr. and Meth.* A**324** (1993) 34; P.P. Allport et al., *Nucl. Instr. and Meth.* A**346** (1994) 479
11. M. Hauschild, *Nucl. Instr. and Meth.* A**379** (1996) 436;
12. T. Sjöstrand, Comp. Phys. Comm. **82** (1994) 74
13. C. Peterson, D. Schlatter, I. Schmitt and P.M. Zerwas, *Phys. Rev.* D**27** (1983) 105. The OPAL parametrisation for JETSET 7.4 is given in OPAL Collab., G. Alexander et al., *Z. Phys.* C**69** (1996) 543
14. G. Altarelli et al., *Nucl. Phys.* B**208** (1982) 365
15. CLEO Collab., S. Henderson et al., *Phys. Rev.* D**45** (1992) 2212
16. The LEP Collabs., ALEPH, DELPHI, L3 and OPAL, *Nucl. Instr. and Meth.* A**378** (1996) 101.
17. OPAL Collab., J. Alexander et al., *Z. Phys.* C**69** (1996) 543
18. J. Allison et al., *Nucl. Instr. and Meth.* A**317** (1992) 47
19. OPAL Collab., R. Akers et al., *Z. Phys.* C**65** (1995) 17
20. OPAL Collab., G. Abbiendi et al., *Eur. Phys. J.* C**8** (1999) 217
21. OPAL Collab., R. Akers et al., *Z. Phys.* C**63** (1994) 197
22. OPAL Collab., P. Acton et al., *Z. Phys.* C**58** (1993) 523
23. OPAL Collab., R. Akers et al., *Z. Phys.* C**66** (1995) 555
24. OPAL Collab., R. Akers et al., *Z. Phys.* C**61** (1994) 209
25. N. Isgur, D. Scora, B. Grinstein and M. Wise, *Phys. Rev.* D**39** (1989) 799
26. P. Collins and T. Spiller, J. Phys. **G 11** (1985) 1289
27. V.G. Kartvelishvili, A.K. Likhoded and V.A. Petrov, *Phys. Lett.* B**78** (1978) 615
28. ALEPH Collab., R. Barate et al., *Eur. Phys. J.* C**5** (1998) 205
29. L3 Collab., M. Acciarri et al., *Phys. Lett.* B**436** (1998) 174. ALEPH Collab., R. Barate et al., *Eur. Phys. J.* C**6** (1999) 555
30. Input Parameters for the LEP Electroweak Heavy Flavour Results for Summer 1998 Conferences, LEPHF 98-01 (see http://www.cern.ch/LEPEWWG/heavy/) used for the Combination of Preliminary Electroweak Measurements and Constraints on the Standard Model, ALEPH, DELPHI, L3 and OPAL collaborations, the LEP Electroweak Working Group, and the SLD Heavy Flavour and Electroweak Groups, CERN-EP/99-015
31. BES Collab., J.Z. Bai et al., *Phys. Rev.* D**58** (1998) 92
32. OPAL Collab., G. Abbiendi et al. *Phys. Lett.* B**444** (1998) 539
33. D. Scora and N. Isgur, *Phys. Rev.* D**52** (1995) 2783
34. D.S. Hwang, C.S. Kim and W. Namgung, *Phys. Rev.* D**54** (1996) 5620